Molecular Neurobiology (2019) 56:1637–1652
https://doi.org/10.1007/s12035-018-1192-8

Cell Death Pathways in Mutant Rhodopsin Rat Models Identifies Genotype-Specific Targets Controlling Retinal Degeneration

Ishaq A. Viringipurampeer[1] · Cheryl Y. Gregory-Evans[1] · Andrew L. Metcalfe[1] · Emran Bashar[1] · Orson L. Moritz[1] · Kevin Gregory-Evans[1]

Received: 26 September 2017 / Accepted: 8 June 2018 / Published online: 18 June 2018

Abstract

Retinitis pigmentosa (RP) is a group of inherited neurological disorders characterized by rod photoreceptor cell death, followed by secondary cone cell death leading to progressive blindness. Currently, there are no viable treatment options for RP. Due to incomplete knowledge of the molecular signaling pathways associated with RP pathogenesis, designing therapeutic strategies remains a challenge. In particular, preventing secondary cone photoreceptor cell loss is a key goal in designing potential therapies. In this study, we identified the main drivers of rod cell death and secondary cone loss in the transgenic S334ter rhodopsin rat model, tested the efficacy of specific cell death inhibitors on retinal function, and compared the effect of combining drugs to target multiple pathways in the S334ter and P23H rhodopsin rat models. The primary driver of early rod cell death in the S334ter model was a caspase-dependent process, whereas cone cell death occurred though RIP3-dependent necroptosis. In comparison, rod cell death in the P23H model was via necroptotic signaling, whereas cone cell loss occurred through inflammasome activation. Combination therapy of four drugs worked better than the individual drugs in the P23H model but not in the S334ter model. These differences imply that treatment modalities need to be tailored for each genotype. Taken together, our data demonstrate that rationally designed genotype-specific drug combinations will be an important requisite to effectively target primary rod cell loss and more importantly secondary cone survival.

Keywords Apoptosis · Necroptosis · Retinal degeneration · Rhodopsin · Neuroprotection · Personalized medicine

Introduction

Genetic retinal diseases are among the most common causes of blindness in the western world. Examples of genetic retinal disease include conditions such as retinitis pigmentosa (RP) and Stargardt's disease. RP has proven to be a genetically heterogeneous form of blindness [1] affecting approximately 1 in 4000 people. Mutations in more than 80 genes have been identified (RetNet; http://sph.uth.tmc.edu/Ret-Net/), with 20 genes associated with the autosomal dominant form of retinitis pigmentosa (adRP). Despite the abundance of available genetic data, there are still no treatments or cures for RP. In 30 to 40% cases of adRP, mutations in the rhodopsin gene are the causative defect [2, 3]. Although mutant rhodopsin ultimately leads to rod photoreceptor cell death, the underlying mechanisms are still incompletely understood. Furthermore, as the rods begin to die, cell death in normal cone photoreceptor cells is initiated, eventually leading to registrable blindness. Since humans rely heavily on their cone-mediated daylight vision, developing a treatment that targets the mechanisms of secondary cone cell death [4] would be a major therapeutic breakthrough, leading to a significant improvement in quality of life in RP patients.

A number of different theories have been proposed to explain secondary cone cell death in rod-mediated RP including nitric oxide release during glia cell activation [5], oxidative stress [6], activation of the insulin/mTOR pathway [7], and a reduction of rod-derived cone viability factor [8]. We recently demonstrated that activation of the inflammasome is also a cause of cone cell death in the P23H model of retinal degeneration [9]. These studies imply that one or more late cell death pathways are upregulated in RP and that which particular pathways are upregulated is genotype-specific. Therefore, precise targeting of these specific pathways would be required to support cone survival.

✉ Kevin Gregory-Evans
kge30@mail.ubc.ca

[1] Department of Ophthalmology and Visual Sciences, University of British Columbia, 2550 Willow Street, Vancouver, BC V5Z 3N9, Canada

Considerable work has been done on developing single-modality (monotherapy) approaches to inhibiting retinal degeneration. The most striking successes to date include anti-VEGF treatment for subretinal neovascularization in AMD [10] and gene therapy for Leber's congenital amaurosis [11]. In contrast, ciliary-derived neurotrophic factor in RP showed no long-term benefits [12]. No intervention has completely halted or significantly reversed vision loss, probably because they target only one of several alternative pathways that, with time, can be bypassed leading to delayed but continual retinal damage [13]. This problem highlights the potential of combination therapy which, by simultaneously targeting multiple pathological pathways, can be designed to overcome different biochemical abnormalities and can be made applicable to many disease phenotypes (genetic or environmental). Such combination therapy is already an essential approach in diseases such as cancer [14], HIV infection [15], hypertension [16], and diabetes [17], where combination regimens have been shown to be invaluable for their synergistic effectiveness, particularly when monotherapy has produced an inadequate response. In the eye, combination therapy is already a major pillar in the management of refractile glaucoma [18] and uveitis [19].

Building on previous studies in animal models and efficacy data from clinical trials, we therefore hypothesize that a cone protective therapy for RP would need to be tailored to the genotype-specific pathological pathways that are activated and most likely in precise combinations. Based on this hypothesis, we compared the effect of a combination of cell death inhibitors in two specific rhodopsin mutants (P23H versus S334ter) that have different underlying pathophysiology. The P23H rat model has a defect in the N-terminal domain of rhodopsin that affects protein folding in the endoplasmic reticulum [20, 21] leading to a relatively slow progression of disease [22] and has been observed in 12% of adRP cases [23]. The S334ter rat model has a defect in the C-terminal region of rhodopsin, which causes a trafficking defect in rhodopsin sorting [24] and a more severe clinical phenotype [25]. We compared the mechanisms of cell death in each model, with the main aim of testing a combinatorial-based approach to protect against photoreceptor degeneration.

Methods

Animals and Drug Administration

Homozygous P23H-line 1 (P23H-1) and S334ter-line 4 (S334ter-4) rhodopsin transgenic rats with similar rates of retinal degeneration were obtained from Professor Matt LaVail, University of California at San Francisco, CA, USA. Pigmented heterozygous P23H-line 1 (P23H) and S334ter-line 4 (S334ter) rats were generated by crossing the original strains to wild-type pigmented Long Evans rats. This was to mimic the autosomal dominant phenotype in humans with a pigmented background and to avoid phototoxicity [26]. All rats were maintained on a 12-h light/dark cycle and were fed and watered ad libitum. Experiments were carried out in accordance with protocols compliant with the Canadian Council on Animal Care and with the approval of the local Animal Care Committee at the University of British Columbia. Both female and male rats were used for these studies. Daily subcutaneous injection of various cell death inhibitors alone or in combination was started at postnatal day 21 (P21) and continued until P120: RIP1 inhibitor (necrostatin-1s), 15 mg/kg (Biovision Inc., Milpitas, CA, USA); poly [ADP-ribose] polymerase (PARP) inhibitor (3-aminobenzamide), 25 mg/kg (Sigma-Aldrich, Oakville, ON, Canada); calpain inhibitor (calpeptin), 250 μg/kg (Sigma-Aldrich, Oakville, ON, Canada); and anti-oxidant and inflammatory inhibitor (*N*-acetylcysteine), 150 mg/kg (Sigma-Aldrich, Oakville, ON, Canada). For controls, rats received daily sham treatments injections of phosphate-buffered saline (PBS).

Antibodies and Lectins

Antibodies used in this study are listed as product number, dilution factor, and application (western blot, WB; immunohistochemistry, IHC). The following primary antibodies were obtained from Sigma-Aldrich (Oakville, ON, Canada): β-actin (A5441, 1:3000, WB), RIPK1 (RIP1) (SAB3500420, 1:500, WB), and RIPK3 (PRS2283, 1:1000, WB); from Abgent (San Diego, CA, USA): RIPK3 (RIP3) (AP7184a, 1:100, IHC); from Cell Signalling (Beverly, MA, USA): cleaved caspase-3 (9661s, 1:1000, WB, 1:200 IHC); from Abcam (Toronto, ON, Canada): IL-1β (ab9722, 1:500, WB), Cd11b (ab8879, 1:200, IHC), and rhodopsin 1D4 (ab5417, 1:500, IHC); from Millipore-Sigma (Etobicoke, ON, Canada): rod arrestin (MAB 5580, 1:300, IHC), M&L opsin (AB5405, 1:300, IHC), and phosphatidylserine clone 1H6 (05–719, 1:100 IHC; 1:500 WB); from Wako (Richmond, VA, USA): Iba1 (019-19741, 1:300, IHC). The following secondary antibodies were used in this study: from Fisher Scientific (Ottawa, ON, Canada): Alexa Fluor® 594 goat anti-mouse IgG (A-11005, 1:200, IHC), Alexa Fluor® 488 goat anti-mouse IgG (A-11001, 1:200, IHC), Alexa Fluor® 488 goat anti-rabbit IgG (A-11008, 1:200, IHC), and Alexa Fluor® 594 goat anti-rabbit IgG (A-11012, 1:200, IHC); from Rockland (Limerick, PA, USA): rabbit antibody IR Dye800 conjugated (611-132-003, 1:15,000, WB) and mouse IgG (H&L) antibody DyLight™ 680 conjugated (610-144-002, 1:15,000, WB). Lectins: FITC-peanut agglutinin (PNA) (Sigma-Aldrich, L7381, 1:50, IHC) was used to identify cone photoreceptors. Wheat germ agglutinin (WGA) (Oregon Green 488 conjugate, Invitrogen, W7024, 1:300, IHC) was used to detect rod photoreceptor outer segments.

Histological Assays

After euthanization by CO_2 and cervical dislocation, the eyes were enucleated and prepared for histology at different postnatal ages (P21–P120) as previously described [27]. In brief, eyes were marked at the 12-o'clock position by leaving a piece of white conjunctival muscle for orientation. The eyes were then immersed in half-strength Karnovsky fixative for 1 h, the anterior segment removed at the ora serrata, the posterior eyecups were embedded in paraffin, and then 5-μm sections (including the optic nerve) were counterstained with hematoxylin and eosin. To account for regional variation of disease progression four 200-μm-long retina images were selected from superior hemisphere peripheral retina (in front of the equator), superior hemisphere central retina (behind the equator), inferior hemisphere peripheral retina, and inferior hemisphere central retina. The two peripheral images were selected approximately two optic disc diameters from the ciliary margin and the two central images the same distance from the edge of the optic nerve head. The sample size was six eyes.

For immunocytochemistry, eyes were fixed with 4% paraformaldehyde (PFA) for 2 h at room temperature (RT) followed by cryoprotection in 30% sucrose overnight, snap frozen, and then embedded in PolyFreeze medium (Polysciences, Warrington, PA, USA). Sagittal cryosections that were ~ 10-μm-thick were incubated overnight at 4 °C with primary antibody diluted in blocking buffer (2% normal goat serum, 0.1% Triton X-100 in PBS). After three washes in PBS-Tween 20 (PBST), sections were incubated for 1 h with secondary antibody diluted in PBS, containing 2% normal goat serum. Nuclei were counterstained with DAPI Fluoromount-G® (SouthernBiotech, Birmingham, AL, USA).

For retinal flatmounts to count cone cells, the anterior segment of the eye was removed after fixation with 4% PFA and then the neuroretina was dissected off the RPE/choroid in one sheet. Neuroretinal tissue was blocked with 3% non-fat dried milk and 0.3% Triton X-100 in PBS for 1 h and then incubated with FITC-conjugated PNA overnight at 4 °C. Samples were washed with PBST three times and the tissue transferred to a microscope slide. Small cuts were made at four opposing points of the tissue so that it could be flattened and then they were mounted using Fluoromount-G®. Immunofluorescent images were acquired using a Zeiss 510 laser scanning confocal microscope, and the cell counts were averaged in six eyes from four areas in the superior, inferior, temporal, and nasal retina, approximately 0.5 mm from the center of the optic nerve using ImageJ software.

The TUNEL procedure and quantification of TUNEL-positive cells were performed on retinal cryosections to detect levels of cell death using an ApopTag® Fluorescein In Situ Apoptosis Detection Kit (Millipore-Sigma, Etobicoke, ON, Canada) according to the manufacturer's instructions. Double staining with microglial marker Iba1 and TUNEL assay was performed as previously described [28].

To examine poly(ADP-ribose) polymerase enzyme activity, an in situ assay was performed as previously described [28]. Briefly, treated and sham-treated retinal cryosections were pre-blocked with an avidin/biotin blocking solution (Vector Laboratories, Burlingame, USA) for 30 min and then incubated for 2 h at 37 °C in a reaction mixture of 100 mM Tris buffer/0.2% Triton X-100 (pH 8.0) that contained 10 mM $MgCl_2$, 1 mM DTT, and 5 μM biotinylated NAD + (Trevigen, Gaithersburg, USA). After 3 × 5 min washes in PBS, the incorporated biotinylated NAD+ was detected by Alexa Fluor 488-conjugated avidin (1:800, 1 h at RT). Images are presented with pseudo-red color as previously reported because the retina has green autofluorescence that impairs image quality.

Western Blots

Fresh neurosensory retinas were dissected and snap frozen in liquid nitrogen and then homogenized by sonication in protein lysis buffer (10 mM Tris base, pH 7.4, 150 mM NaCl, 1 mM EDTA, 1 mM EGTA, 1% Triton X-100, 0.5% NP-40) and supplemented with protease/phosphatase inhibitor cocktail (Cell Signalling, Beverly, MA, USA). Total protein concentration was determined using the DC protein assay (Bio-Rad, Hercules, CA, USA). Protein samples (40 μg) were mixed with sample buffer, boiled for 10 min, separated by SDS-polyacrylamide gel electrophoresis, and then transferred to Immobilon-FL membrane (Millipore Sigma, Etobicoke, ON, Canada). Membranes were blocked in 5% non-fat milk powder in PBS/0.1% Tween-20 (PBST) for 1 h at RT and incubated overnight at 4 °C with appropriate primary antibody in the blocking buffer. Following three washes in PBST, the membranes were incubated in the dark for 1 h at RT with appropriate fluorescent secondary antibody (IRDye 800 or IRDye 680). The membranes were then washed three times in PBST in the dark and protein bands were visualized using a Li-COR Odyssey detector (Mandel Scientific, Guelph, ON, Canada). ImageJ software was used to analyze band intensities relative to loading control (β-actin). Western blots were repeated three times using tissues from independent animals.

RNA Extraction, RT-PCR, and Semi-Quantitative Real-Time PCR

Briefly, total RNA was isolated from neurosensory retinas using Aurum™ Total RNA Mini Kit (Bio-Rad Laboratories; Hercules, CA) according to the manufacturer's instructions and RNA was quantified by NanoDrop spectrometry (ThermoScientific, Wilmington, DE, USA). Starting with 200 ng of total RNA, reverse transcription was performed using the QuantiTect Reverse Transcription Kit (Qiagen, Toronto, ON, Canada) and relative gene expression of *Hmgb1* (Rn02377062_g1), *Il-1α*

(Rn00566700_m1), and *Gapdh* (Rn01775763_g1) was quantified using the TaqMan primer and labelled probe protocol with a ViiA 7 Real-Time PCR system (Applied Biosystems, Burlington, ON, Canada) as previously reported [9]. Real-time PCR data were analyzed by the comparative C_T method [29]. Each reaction was undertaken on three occasions, and for each of these, individual samples were subdivided into three aliquots for measurement.

Electroretinography

Rats were dark-adapted overnight prior to electroretinogram (ERG) analysis, then general anesthesia was induced with intraperitoneal ketamine plus xylazine and rats then placed on a heating pad to maintain a constant body temperature at 37 °C during the entire test. The cornea was anesthetized with topical 0.5% proparacaine hydrochloride (Bausch and Lomb, Rochester, NY) and the pupils were dilated with 2.5% phenylephrine and 1% atropine. A drop of 2% hydroxypropyl methylcellulose was placed on each cornea to maintain corneal hydration. ERG responses of the retina to light flashes were recorded using an Espion E2 system with a Colordome mini-Ganzfeld stimulator (Diagnosys LLC, Lowell, MA, USA) at P21, P45, P90, and P120 by averaging 15 responses at a stimulus intensity of 3.16 cd s/m^2. Light-adapted cone responses were carried out in 30 cd/m^2 background light at a 30-Hz flicker frequency. The sample size was ten for all cohorts for the monotherapy and combination therapeutic experiments.

Statistical Analysis

For assessment of outer nuclear layer (ONL) thickness, an unpaired two-tailed Student's *t* test was used for comparisons between treated and untreated groups. *P* values less than 0.05 were considered significant. For the analysis of TUNEL-positive cells, semi-quantitative RT-PCR and western blot, one-way analysis of variance followed by post hoc Tukey's test was used. For ERG analyses, multiple group comparison was performed by one-way or two-way ANOVA followed by Tukey-Kramer adjustments. Differences were considered significant at $P < 0.05$. Results are reported as mean ± SEM. All statistics were performed in either the GraphPad Prism 5.0 or online statistic tools (ANOVA).

Results

Activation of Cell Death Pathways in S334ter Compared to P23H Models

To compare the spatiotemporal activation of photoreceptor cell death pathways in the two models with similar rates of retinal degeneration on a pigmented background, immunostaining of retinal sections was carried out for a number of cell death markers. Differential staining was observed with caspase-3 (cCASP-3, detecting caspase-dependent apoptosis [30]) and receptor interacting kinase 3 (RIP3, detecting necroptosis [31]) at early stages of retinal degeneration. At P21, many caspase-3-positive photoreceptor cells were apparent in the ONL of the S334ter retina compared to P23H (Fig. 1a–c). At both P45 and P120, caspase-positive cells were observed in the S334ter ONL (Fig. 1e, n) compared to very few in the P23H retina (Fig. 1f, o). However, there were caspase-positive cells in the inner nuclear layer (INL) of the P23H retina at P120 (Fig. 1o). Co-localization of RIP3 staining and 1D4 (a rhodopsin marker labelling wild-type rod photoreceptors) was detected at all three time points in the P23H retina (Fig. 1i–r), but we saw no RIP3 staining in S334ter retina at P21 or P45 (Fig. 1h, k). At P120, there was RIP3 signal in the S334ter retina (Fig. 1q); however, this was found to co-localize with peanut agglutinin, a marker for cone photoreceptors (Fig. 1s). These spatiotemporal differences were quantified by western blot analysis (Fig. 2a–c). In S334ter whole retinal extracts at P21 and P45, there was abundant expression of cCASP-3 that was absent in the P23H retina (Fig. 2a, b), mirroring the immunohistochemistry data. At P120, cCASP-3 was detected in retinal extracts from both models. In P23H retinal extracts, RIP3 expression increased over background levels in wild-type rats at P21, P45, and P120. In the S334ter retinal extracts, there was no expression of RIP3 at P21, whereas at P45 and P120, RIP3 was increased. These results suggest that rod photoreceptor degeneration in the S334ter model is initially mediated via caspase-dependent apoptosis, whereas cone cell death occurs through necroptosis. Conversely, rod photoreceptors in the P23H retina die via RIP3-dependent necroptosis, whereas cones in this model die by inflammasome activation as we previously reported [9].

The expression of PARP was tested as it is a marker of caspase-independent apoptosis [28] and expression of RIP1 was also assessed as it is required for both caspase-dependent and caspase-independent cell death mechanisms [31]. Using an in situ assay to measure PARP activity directly, we found very little PARP activity in wild-type retinal sections, whereas in the S334ter retina, high levels of PARP activity were present in the ONL and INL at all time points tested (Fig. 2d). In the P23H retina, there was relatively less PARP activity compared to the S334ter retina. When S334ter rats were treated with 3AB (an inhibitor of PARP), the levels of PARP activity at P45 and P120 were greatly reduced. Western blot demonstrated the ubiquitous expression of RIP1 in wild-type retina and in both models at all time points (Fig. 3a). Previously we demonstrated that a variety of inflammatory molecules were released by stress and by dying photoreceptors in the P23H model including IL-1α and IL-1β [9]. In the S334ter model, inflammatory cytokines appeared to be

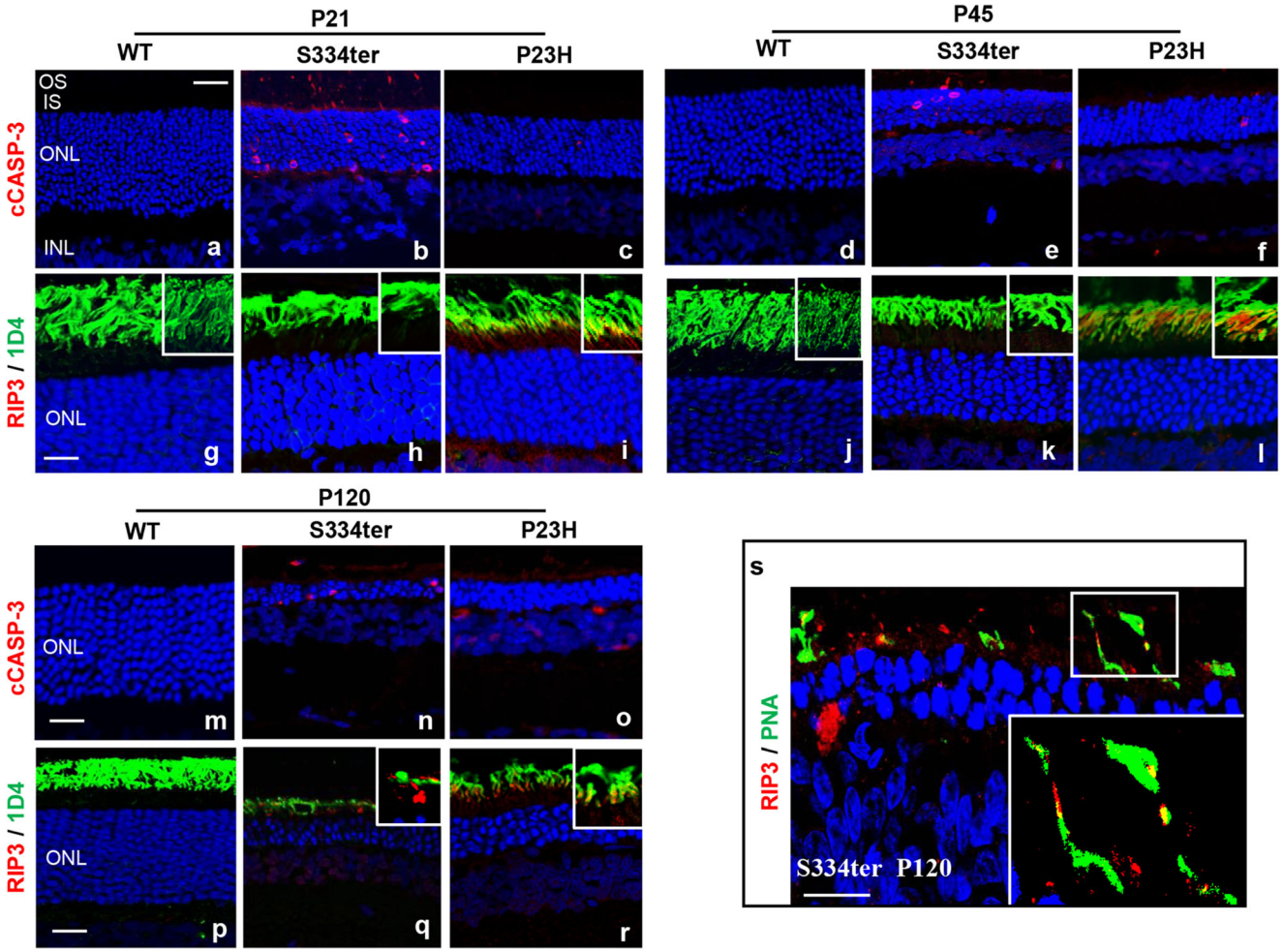

Fig. 1 Differential cell death pathway activation in P23H and S334ter photoreceptor degeneration. **a**–**f** Labelling of cCASP3-positive (red) photoreceptor nuclei in the outer nuclear layer (ONL) of retinal sections at P21 and P45. OS, outer segments; IS, inner segments; INL, inner nuclear layer. Scale bar = 25 μm. **g**–**l** RIP3 (red) co-localizes with wild-type rhodopsin (green) in P23H retina but not in S334ter retina at P21 and P45. Scale bar = 10 μm. Inset: higher magnification of co-localization. **m**–**o** Labelling of cCASP3-positive (red) photoreceptor nuclei in the ONL of retinal sections at P120. Scale bar = 10 μm. **p**–**r** RIP3 (red) co-localizes with rhodopsin (green) in P23H retina but not in S334ter retina at P120. Scale bar = 10 μm. **s** RIP3 co-localizes with peanut agglutinin (green), a marker for cone photoreceptors in S334ter retina at P120. Scale bar = 10 μm. Inset: higher magnification of co-localization. All retinal sections counterstained with DAPI

less important. For example, although the IL-1β precursor was expressed as would be expected in both models, the mature form of IL-1β was more than twofold higher in the P23H retina compared to the S334ter retina. (Fig. 3b, d). Quantitative RT-PCR revealed a fourfold change in transcript levels of IL-1α in P23H retina compared to S334ter at P120 (Fig. 3c). These data demonstrate that more than one cell death pathway is activated in each model, and the pathways are different in each model.

Comparison of Microglial Infiltration in S334ter and P23H Models

Recent evidence suggests that in some disease states non-cell autonomous inflammatory mechanisms exacerbate neuronal degeneration [32]. For example, in the rd10 (*Pde6b*) mouse model of retinal disease, microglia infiltrate the ONL not only to clear dead photoreceptors but can also kill live photoreceptors directly [33]. This phenomenon occurs because dead or stressed photoreceptor cells express phosphatidylserine (PS) on their surface making them phagocytic targets for microglia [32]. Therefore, we assessed the distribution of retinal microglia in both retinal degeneration models. Surprisingly, many more infiltrating microglia labelled with Iba1 antibody were present in the ONL of S334ter retina compared to P23H retina at P120 (Fig. 4a), and this difference was maintained during the time course of photoreceptor degeneration (Fig. 4b). Double-labelling of retinal sections at P120 with Iba1 and rod photoreceptor-specific arrestin revealed active engulfment of dying rods by microglia in the S334ter retina but not in P23H retina (Fig. 4c). Conversely, labelling of activated microglia with Cd11b and ML cone opsin at P120 demonstrated

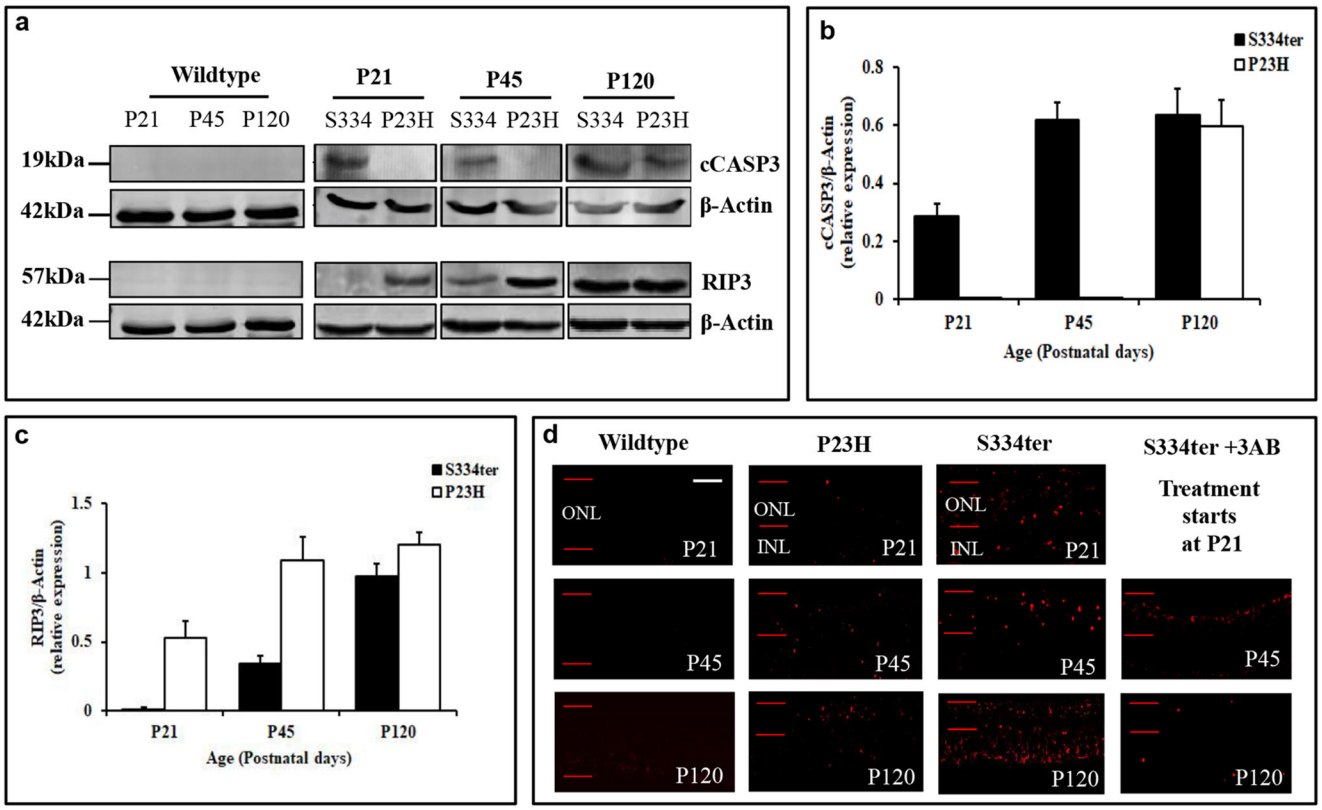

Fig. 2 Retinal expression of cell death markers in P23H and S334ter rats. **a** Representative western blot showing temporal expression of cCASP-3 and RIP3 from whole retinal extracts. Protein loading control, β-actin. Blots are representative of three independent experiments. **b** Quantitation of cCASP3 expression relative to β-actin. **c** Quantitation of RIP3 expression relative to β-actin. **d** Spatiotemporal localization of in situ PARP enzyme activity (red) in retinal cryosections. S334ter animals were treated with 3AB, an inhibitor of PARP activity. White scale bar = 10 μm. Red bars indicate the limits of the ONL. There is no image of S334ter at P21 with treatment as this is when treatment begins

active engulfment of cones in the P23H retina but not S334ter retina (Fig. 4c). Immunohistochemistry revealed expression of phosphorylated PS in photoreceptor somata in both P23H and S334ter retinas (Fig. 4d) similar to that reported in the *rd10* mouse [33] and was confirmed by western blotting (Fig. 4e), suggesting that microglial phagocytosis actively contributed to the demise of live photoreceptors.

Mono-Therapeutic Approaches to Protect S334ter-Mediated Photoreceptor Degeneration

The specific cell death pathways that we found to be activated in the S334ter model were targeted by potent cell death inhibitors including calpeptin (an inhibitor of calpain involved in caspase-independent cell death); 3-aminobenzamide (3AB, a PARP inhibitor); necrostatin-1s (Nec-1s, a RIP1 inhibitor), and *N*-acetylcysteine (NAC, an anti-oxidant/anti-inflammatory drug). Efficacy of the inhibitors was tested by histology and effect on visual function via electroretinography (ERG) at the following time points: P21, P45, P90, and P120. In the sham-treated S334ter rats at P120, histology from central retinal locations revealed that two to three rows of photoreceptor nuclei remained in the ONL (wild-type rats have 10–12 rows), whereas treatment with four to five rows of nuclei (Fig. 5a). Photoreceptor outer segments were absent in the sham-treated retinas, whereas treatment with 3AB resulted in clear preservation of outer segments. This corresponded to reduced PARP activity when S334ter rats were treated with 3AB (Fig. 2d). A more rigorous comparison was made to compare the number of photoreceptor nuclei in the ONL at four standardized regions the retina (see "Methods") and the mean of photoreceptor counts was plotted for each inhibitor (Fig. 5b). Compared to sham-treated rats, only treatment with 3AB resulted in significant preservation of photoreceptors at P120 ($P < 0.0001$, $n = 6$).

Retinal function was assessed by scotopic and 30 Hz flicker ERG responses (Fig. 5c). Rod photoreceptor function measured by the scotopic b-wave amplitude response at P21 in sham-treated rats was already reduced by ~25% from wild-type levels (475 μV versus normal maximum scotopic b-wave amplitude of ~625 μV) and was followed by a gradual decline over time to ~225 μV at P120 (Fig. 5d). At P120, the b-wave amplitudes were between 50 and 100 μV higher with NAC, calpeptin, and 3AB compared to sham-treated controls. Statistical differences between multiple group were assessed by two-way ANOVA on the five S334ter groups ($n = 10$). This

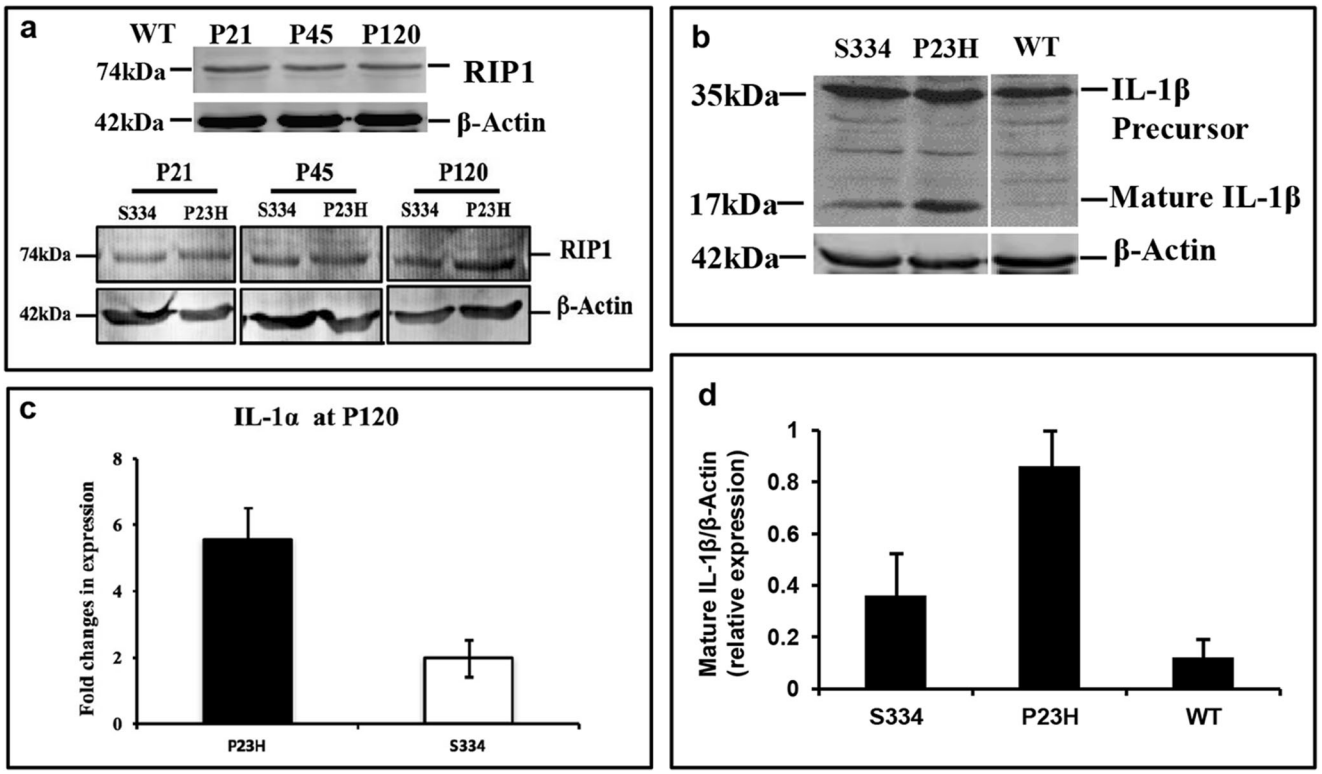

Fig. 3 Comparative inflammatory marker expression in S334ter and P23H retina. **a** Western blot showing temporal expression of RIP1 from whole retinal extracts. Protein loading control, β-Actin. Blots are representative of three independent experiments. **b** Western blot showing expression of mature IL-1β and its precursor in whole retinal extracts at P120. Protein loading control, β-Actin. Blots are representative of three independent experiments. **c** Quantitative RT-PCR analysis of IL-1α expression from total RNA retinal extracts at P120. Data plotted as mean fold change in expression ± SEM ($n = 3$). **d** Quantitation of IL-1β relative to β-actin from western blot in **b**

showed significant effects of time ($P = 0.0001$) and treatment ($P = 0.01$). Post hoc (Tukey) comparisons between treatment groups showed significant effects of calpeptin versus sham ($P < 0.001$), 3AB versus sham ($P < 0.001$), and NAC versus sham ($P < 0.001$).

The secondary effect of the rod photoreceptor-specific S334ter mutation on cone cell viability was assessed by histology and electrophysiology. Whole-mount immunofluorescence for cone-specific PNA demonstrated that treatment with either Nec-1s ($P < 0.003$) or NAC ($P < 0.05$) supported significantly more cone survival compared to sham-treated eyes ($n = 10$) (Fig. 6a, b). Cone function in vivo was measured by the 30-Hz flicker component from the electroretinography testing (Fig. 5c). Both Nec-1s and NAC showed consistently a significantly higher 30 Hz flicker amplitude compared to the other drug treatments over time (Fig. 6c). Statistical differences were assessed using two-way ANOVA and showed significant effects of time ($P = 0.0001$) and treatment ($P = 0.0001$). Post hoc (Tukey) comparisons between treatment groups showed significant effects of Nec-1s versus sham ($P < 0.001$) and NAC versus sham ($P < 0.001$). Relative to the wild-type 30-Hz amplitudes denoting the maximal response (100%), the untreated amplitudes were approximately 63% of wild-type, whereas Nec-1s was 74% and NAC 77% of wild-type, representing an 11 and 14% preservation of the cone response, respectively.

Efficacy of Combined Drug Treatment on P23H and S334ter Retinal Degeneration

Since a number of different cell death pathways were activated in each of the rat models, we reasoned that a combination of drugs may improve the protective effect we had observed with monotherapies. All animals were treated daily with a combination of cell death inhibitors (Calpeptin+3AB+Nec-1s+NAC) by subcutaneous injection from P21 to P120. Histological examination at P120 revealed that combination therapy in P23H animals resulted in a thicker ONL and well-formed outer segments compared to sham-treated retina (Fig. 7a). However, combination therapy in the S334ter rats had a more modest effect on the retina. These qualitative observations were confirmed by counting photoreceptor nuclei in the ONL at four specific coordinates in the retina (Fig. 7b), demonstrating a significant benefit to the P23H retina in all four regions ($P < 0.001$, $n = 6$). In addition, the length of the rod photoreceptor OS was measured after immunohistochemical staining of retinal cryosections with wheat germ agglutinin which labels rod photoreceptor OS (Fig. 7c). In the sham-

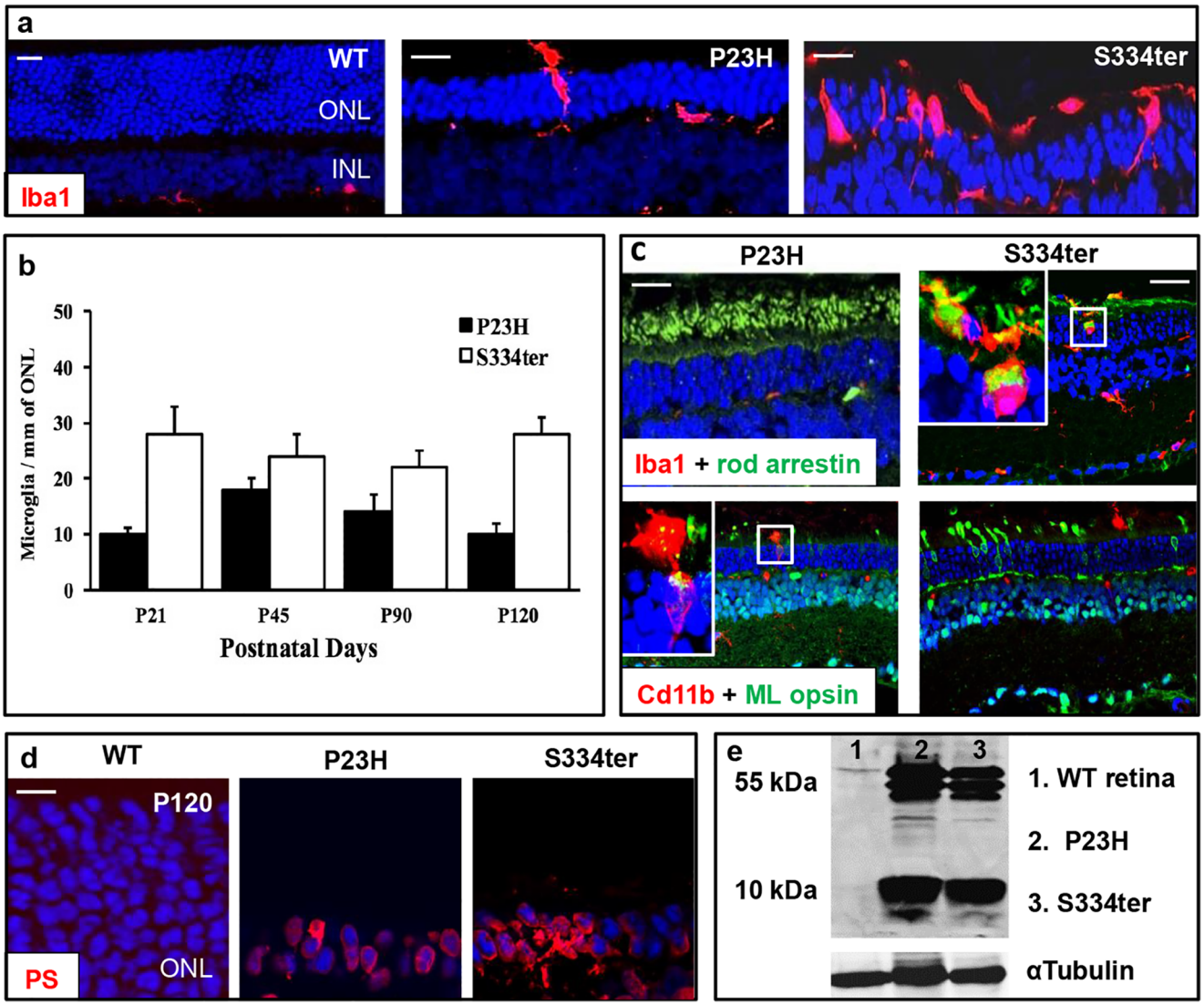

Fig. 4 Microglial infiltration in degenerating P23H and S334ter retina. **a** Retinal sections from wild-type (WT), P23H, and S334ter at P120 labelled with Iba1 antibody (red) detecting activated microglia. Scale bar = 10 μm. **b** Number of microglia per millimeter in the ONL of the retina relative to the time course of degeneration. **c** Upper panels: co-localization of microglial marker Iba1 (red) and the rod photoreceptor-specific marker arrestin (green). Inset: higher magnification of engulfed rod photoreceptor in S334ter retina. Lower panels: co-localization of microglial marker Cd11b (red) and the cone photoreceptor-specific marker ML opsin (green). Inset: higher magnification of engulfed cone photoreceptor in P23H retina. Scale bar = 10 μm. **d** Localization of phosphatidylserine (PS) in red to photoreceptors in the ONL of mutant retina compared to WT at P120. Scale bar = 10 μm. **e** Western blot showing expression of PS in P23H and S334ter mutant retina from whole retinal extracts compared to WT. Protein loading control, β-actin. Blots are representative of three independent experiments

treated retina, the OS length in P23H was 5.5 ± 2 μm and in S334ter 3.5 ± 3 μm, whereas after combination therapy, the OS length was significantly larger in P23H (20 ± 4 μm, $P < 0.001$) and in S334ter retina (10 ± 3 μm, $P < 0.05$) (Fig. 7c). In comparison, the OS length of wild-type photoreceptors was 39 ± 2 μm.

The 30-Hz flicker amplitudes measuring the cone responses of the retina (Fig. 8a, b) revealed a significant protective effect when P23H animals were treated with combination therapy (19 ± 2 μV) compared to sham-treated controls (12 ± 3 μV) at P120 ($P < 0.05$, $n = 10$). In comparison to maximal wild-type amplitudes (100%) at P120, the 30-Hz amplitudes in sham-treated P23H retinas were only 42% of wild-type, whereas treated P23H retinas had amplitudes that were 67% of wild-type, representing a 25% preservation of cone response. However, combination therapy in the S334ter did prevent not significantly protect against the reduction in cone function ($P > 0.20$, $n = 10$). Whole-mount PNA staining showed an increase in the density of cones in both P23H- and S334ter-treated retinas compared to sham-treated controls, although this did not reach statistical significance in the S334ter retinas because there were more cones present in the sham-treated retinas (Fig. 8c, d). This may reflect the 5–10-μV higher 30 Hz amplitudes in the sham-treated S334ter

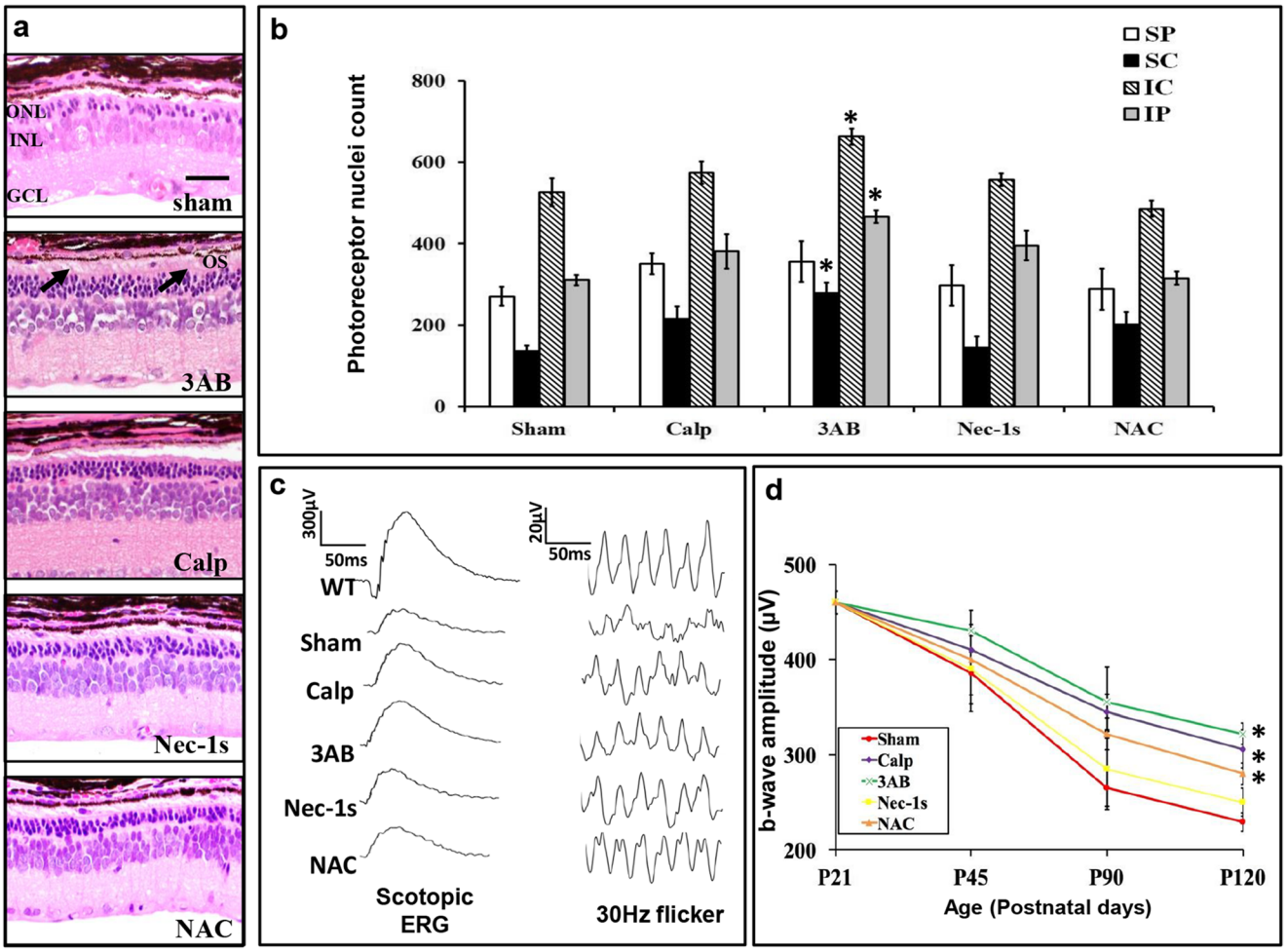

Fig. 5 Efficacy of monotherapies on retinal degeneration in the S334ter rat retina. **a** Hematoxylin & eosin (H&E) stained sagittal sections through central retina at P120 in S334ter rats that were treated with 3AB, Calp, Nec-1s, and NAC compared to sham-treated controls. ONL, photoreceptor outer nuclear layer; INL, inner nuclear layer; GCL, ganglion cell layer. Arrows pointing to photoreceptor outer segments (OS). White scale bar = 50 μm. **b** Average photoreceptor nuclei counts for each treatment in four standardized retinal regions: SP, superior peripheral; SC, superior central; IC, inferior central; IP, inferior peripheral. Data presented as mean ± SEM ($n = 6$). Student's t test, $^*P < 0.001$. **c** Representative scotopic and 30-Hz flicker ERG waveforms at P120 for each drug treatment. **d** Temporal comparison of b-wave amplitudes from ERG data for each drug treatment. Data plotted as mean ± SEM ($n = 10$). Two-way ANOVA revealed significant effects for calpeptin ($^*P < 0.001$), 3AB ($^*P < 0.001$), and NAC ($^*P < 0.001$) compared to sham-treated rats

retinas from P45 to P120 compared to P23H as there were more cones present contributing to the response (Fig. 8a).

Discussion

Through histological, biochemical, and functional studies, the cell death pathways in the S334ter model of retinal degeneration were compared to previously reported data for P23H model, and the effects of inhibiting these pathways alone or in combination were assessed. In the S334ter model, caspase-dependent cell death was a primary driver for early rod photoreceptor cell death concurring with previous reports [34, 35], whereas cone cell death occurred through RIP3-dependent necroptosis. Conversely, we previously reported that necroptotic-mediated signalling was the main driver of rod cell death in the P23H model, whereas activation of the NLRP3 inflammasome was the mechanism for secondary cone cell death [9]. The activation of different photoreceptor cell-specific death mechanisms is echoed in other animal models such as the *rd10* mouse (*Pde6b* mutation) where rods die through a caspase-independent apoptotic mechanism, whereas secondary cone cell death occurs via necroptosis [35, 36]. In another model ($Irbp^{-/-}$ mouse), apoptotic cell death occurred early in rods, whereas necroptosis was the main driver of progressive rod and cone degeneration [37]. Furthermore, in the $pde6c^{-/-}$ zebrafish model of achromatopsia, primary cell death in cones occurs via necroptosis with secondary rod cell death occurring through a caspase-dependent mechanism [38]. Because each model has activation of different cell death mechanisms, this implies that treatment modalities using more than one drug might need

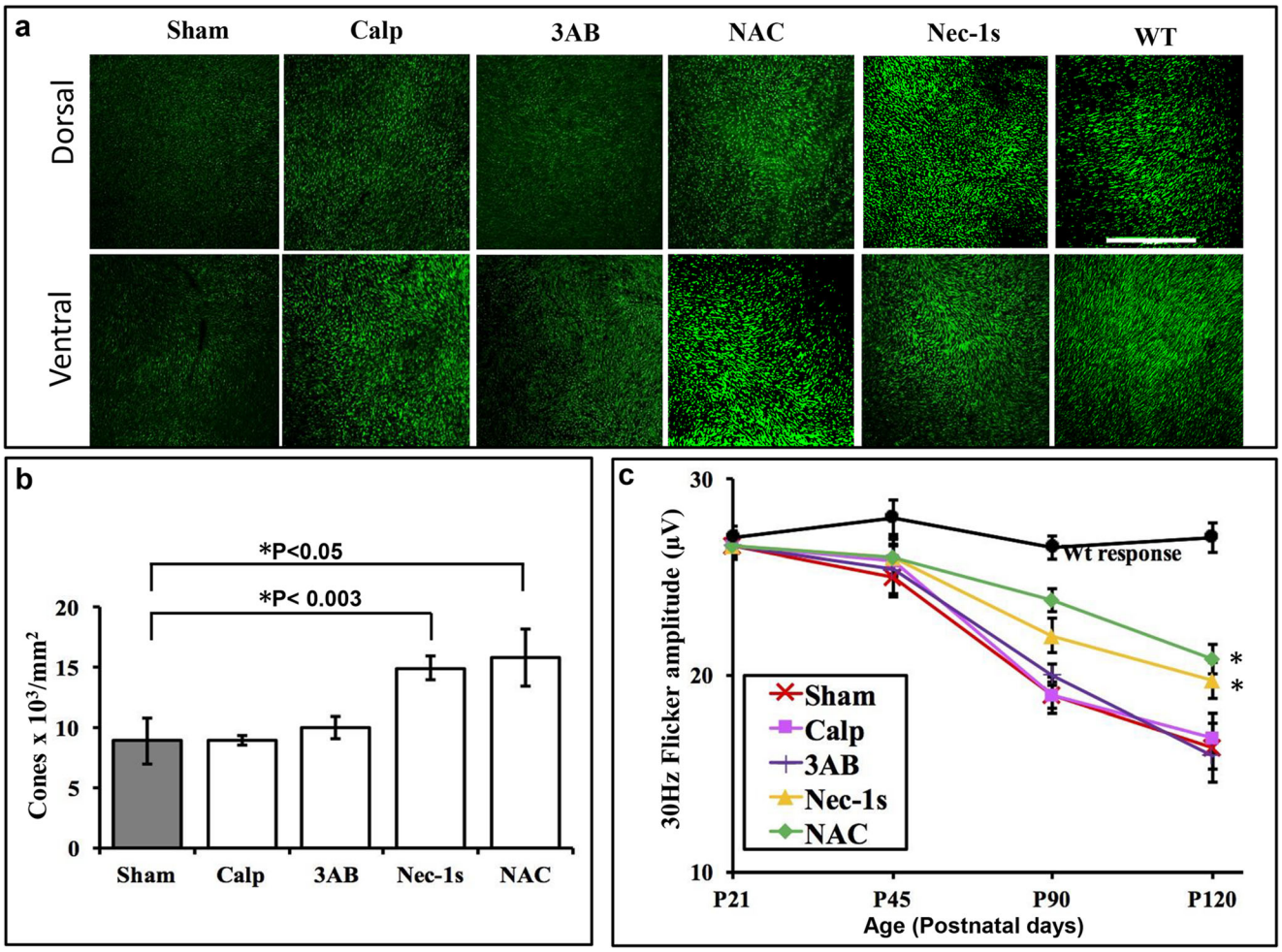

Fig. 6 Effect of monodrug therapy on cone photoreceptor survival. **a** PNA-labelling of cones in retinal flatmounts at P120 that were treated with Calp, 3AB, Nec-1s, and NAC compared to sham-treated and wild-type samples. Representative images taken from central dorsal and ventral retina. White bar = 500 μm. **b** Quantification of PNA-labelled cones determined from flatmounts from four retinal areas. Data presented as mean ± SEM ($n = 10$). Asterisk: statistical significance was determined using Student's t test. **c** Comparison of 30 Hz flicker amplitudes with the different drug treatments compared to sham-treated and wild-type control responses. Statistical significance was determined by two-way ANOVA comparing each treatment with sham-treated rats. *$P < 0.001$ ($n = 10$)

to be tailored for each genotype (Table 1). This may explain why only a modest level of neuroprotection has been observed in animal models and in patients enrolled in clinical trials with use of a single drug [11, 13, 44–46].

Based on the results we obtained for the effect of individual drug inhibitors on preservation of vision, we reasoned that a combination of drugs might have a synergistic effect. When assessing the same outcome efficacy parameters, it was surprising that the combination therapy was consistently equivalent or had a better effect than the best individual drug alone in P23H model, whereas in the S334ter model, the combined therapy was the same or worse than the best individual drug alone (Table 2). For example, the ERG b-wave amplitudes in P23H with single drugs ranged from 50 to 80 μV better than untreated, whereas combination therapy produced a 100-μV increase in amplitude. Conversely, in the S334ter model, single drugs ranged from a 50- to 100-μV increase in amplitude, whereas combination therapy resulted in only a 35-μV increase in amplitude. Similarly, the change in cone density followed the same pattern of efficacy: combination therapy resulted in lower cone survival than individual drugs in the S334ter model but higher cone survival than individual drugs in the P23H model. These comparisons reveal that combining drugs does not necessarily improve the outcome over monotherapy but can make it worse than just using a single drug. This might occur due to the mechanism of action of the mutation (in P23H, mis-folding; in S334ter, mis-localization). For instance, it could be that in the P23H retina that if a drug could simply improve folding then the protein could be trafficked correctly to the outer segment where it would function correctly. This might be more easily overcome than in the S334ter retina where the protein is in the wrong place. Another explanation for worse efficacy with combination drugs in the S334ter retina might be because inhibiting one

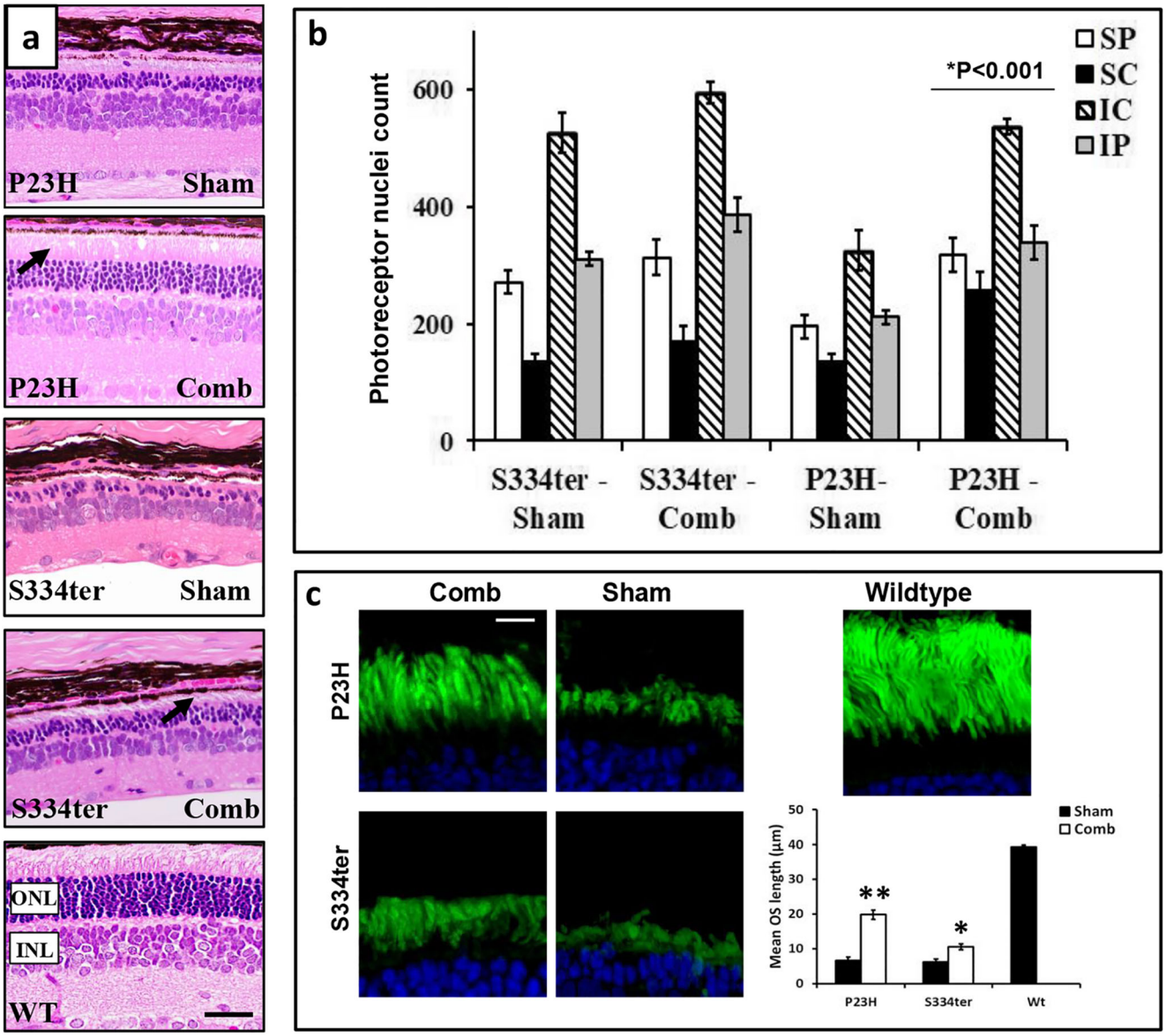

Fig. 7 Effect of combination therapy on retinal degeneration. **a** Representative H&E stained sagittal sections through central retina at P120 in P23H and S334ter rats that were treated with combination therapy compared to sham-treated controls. Wild-type section (WT) showing normal retinal lamination. ONL, photoreceptor outer nuclear layer; INL, inner nuclear layer; GCL. Arrows pointing to photoreceptor outer segments. Scale bar = 50 μm. **b** Average photoreceptor nuclei counts for each combination (Comb) treatment versus sham injection in four standardized retinal regions: SP, superior peripheral; SC, superior central; IC, inferior central; IP, inferior peripheral. Data presented as mean ± SEM ($n = 6$). Student's t test, $^*P < 0.001$. **c** Comparison of the immunochemical localization of WGA (green) in the retina of treated, untreated and wild-type rats at P120. Scale bar = 10 μm. The histogram compares the OS length. Data presented as mean ± SEM ($n = 10$). Student's t test, $^*P < 0.005$; $^{**}P < 0.001$

mechanism might limit the efficacy of inhibiting another, because compensatory or parallel pathways might be activated. For example, inhibiting caspase-dependent apoptosis with an inhibitor of caspase-8 leads to activation of the alternative necroptotic pathway thereby increasing cell death [47] and inhibition of caspase-8 can also cause an inflammatory response [48]. This raises the issue of whether it is better to treat rhodopsin-RP patients with a more generalized combination therapy (which would have the potential for multiple genotype applications) or if specific combinations may be required.

The combination therapy data in the P23H model confirms that limiting both the inflammasome-driven response in cones and necroptotic signaling in rods represents a rationale therapeutic design for this specific genotype. As P23H is the commonest mutation found in North America in patients with dominant RP [23], then a therapeutic strategy to prevent both rod, but more importantly cone cell loss, could be relevant to many patients. One question that arises however in these types of studies is how relevant are the animal models to the human disorders when designing treatment strategies? Both P23H

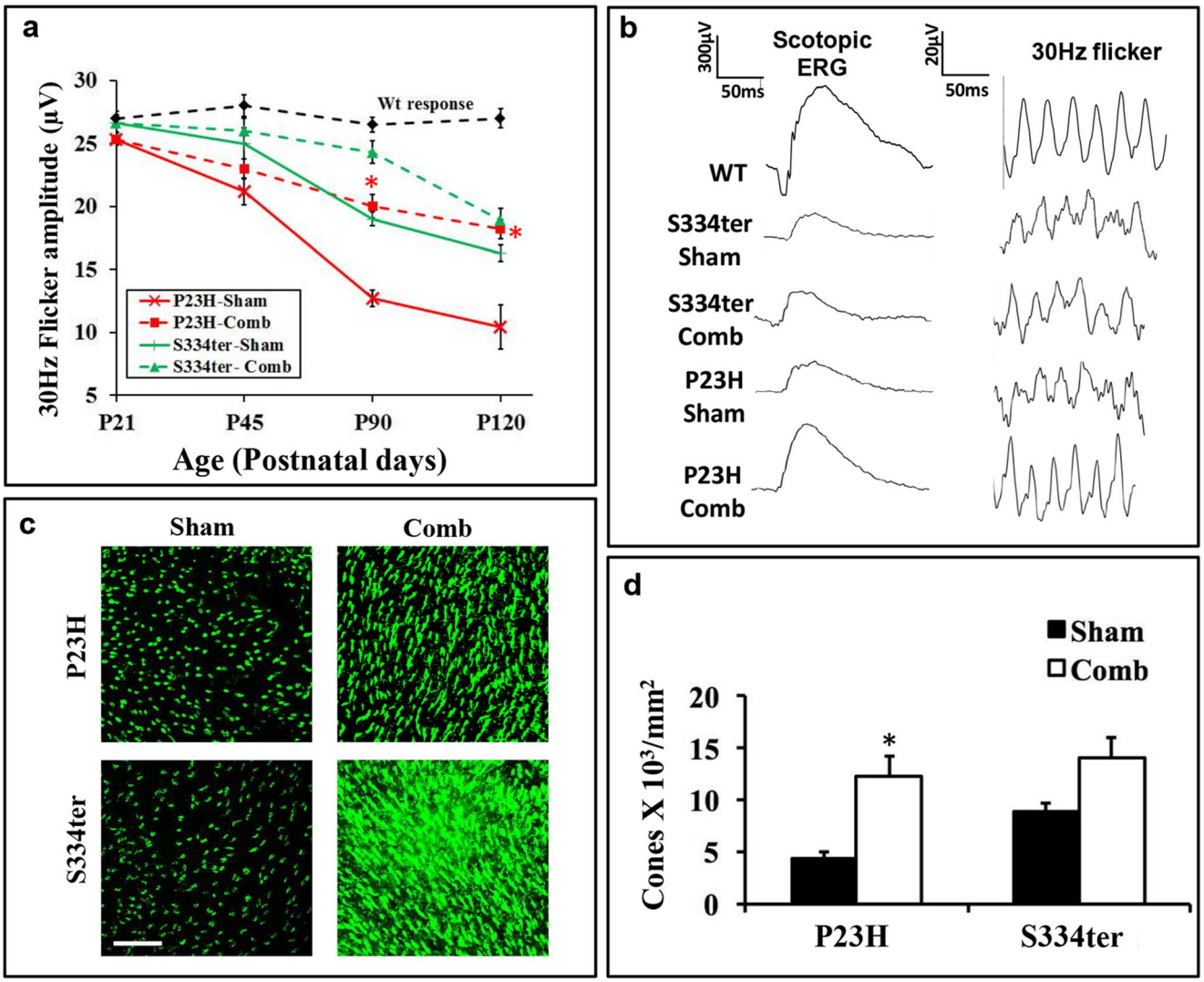

Fig. 8 Effect of combination therapy on cone photoreceptor survival in P23H and S334ter rats. **a** Thirty-Hertz flicker amplitudes in P23H (red lines), S334ter (green lines), and wild-type eyes (black line) that were either treated or untreated. At P90 and P120, P23H rats treated with combination therapy had significantly larger amplitudes, determined by two-way ANOVA. Red (asterisk), $P < 0.001$ ($n = 10$). **b** Representative scotopic and 30 Hz flicker ERG waveforms at P120 with either combination or sham treatment. **c** PNA-labelling of cones (green) in retinal whole-mounts at P120 that were treated with combination therapy or sham injections. Scale bar = 50 μm. **d** Quantification of PNA-labelled cones determined from whole mounts in **c**. Data presented as mean ± SEM ($n = 10$). Student's *t* test (asterisk), $P < 0.05$

and S334ter lines were generated by inserting the relevant mutant mouse whole rhodopsin genomic transgene onto the wild-type rat background. The P23H-line 1 model has nine copies of the transgene; however, transcriptional silencing is thought to occur because mutant P23H only represents 43% of all rhodopsin transcripts present [49]. This is what is predicted in the human condition where equivalent amounts of wild-type and mutant rhodopsin would be expressed. In the P23H mouse knock-in model that recapitulates the heterozygous human mutation [50], inhibiting the inflammasome also prevented cone cell loss [9]. This provides evidence that the therapeutic results obtained in the P23H transgenic model regarding cone survival are conserved across species and models and therefore likely to be relevant to therapeutic outcomes in human patients. In the S334ter-line 4 model, the transgenic rhodopsin is present at about 10% of the level of the endogenous rhodopsin and causes mis-sorting of the mutant truncated rhodopsin to the rod photoreceptor [24]. This pathophysiology is corroborated in other models where there is a similar C-terminal rhodopsin truncation abnormality [51, 52] and in a Q344ter knock-in mutation recapitulating a known human mutation on a heterozygous wild-type rhodopsin background [53, 54]. This suggests that the therapies tested in S334ter rat model could be directly relevant to future testing in human RP.

The role of microglia in retinal degeneration is somewhat controversial and is dependent on genotype and phenotype. The initiation of photoreceptor cell death leading to the

Table 1 Photoreceptor-specific cell death mechanisms in different animal models

Model	Main driver of rod cell death	Main driver of cone cell death	Example of drug combinations
Rho S334ter rat	Caspase 3-dependent [this paper, 34–35]	Necroptosis (RIP1/3) [this paper]	zVAD-fmk for rods Nec-1s for cones
Rho P23H rat	Necroptosis (RIP1/3) [9]	NLRP3 inflammasome [9]	Nec-1s for rods *N*-acetylcysteine for cones
Rho P23H mouse	Necroptosis (RIP1/3) [9]	NLRP3 inflammasome [9]	Nec-1s for rods *N*-acetylcysteine for cones
Pde6b (Rd10) mouse	Caspase-independent [35]	Necroptosis (RIP1/3) [36]	Calpain inhibitor for rods Nec-1s for cones
Irbp KO mouse	Necroptosis (RIP1/3) and caspase-3 apoptosis [37] (rod/cones not differentiated)		Nec-1s and zVAD-fmk for both rods and cones
pde6c KO zebrafish	Caspase 3-dependent [38]	Necroptosis (RIP1/3) [38]	zVAD-fmk for rods Nec-1s for cones
Mertk (RCS) rat	Caspase-independent release of AIF [39] and caspase-3 activation in photoreceptors [40] (rod/cones not differentiated)		Calpain to inhibit AIF and Y-27632 to inhibit ROCK/caspase-3
Pde6b (Rd1) mouse	Caspase-independent release of AIF [41]	Caspase-3 apoptosis [42, 43]	Calpain to inhibit AIF in rods and TUDCA in cones

References in square brackets. Possible drug combinations for each genotype targeting the main drivers of cell death

activation and migration of microglia to phagocytose dying photoreceptors and thereby eliminates damaging cellular debris could be considered as a pro-survival mechanism [33, 55–57]. However, independent of this activity, there are several reports demonstrating photoreceptor rescue in inherited retinal degeneration by inhibition of microglial cell activity

Table 2 Compilation of cell death and treatment data from this paper and from previous work in these models at P120 (9)

Assessment parameter	S334ter	P23H
Specific cell death marker activation	Caspase-3 PARP RIP1	RIP3/RIP1 NLRP3 IL-1α/IL-1β
Monotherapy: Δ microglia	**NAC**>Nec-1s/3AB/Calp (28 → 13 microglia/mm, 54% ↓)	**NAC/Nec-1s**>3AB/Calp (10 → 2.5 microglia/mm, 75% ↓)
Combination: Δ microglia	Similar decrease in microglia (28 → 12 microglia/mm, 57% ↓)	Similar decrease in microglia (10 → 3 microglia/mm, 70% ↓)
Monotherapy: Δ histology	**3AB**>Calp/Nec-1s/NAC (19 → 25 μm ONL thickness)	**Calp/Nec-1s/NAC**>3AB (15 → 25 μm ONL thickness)
Combination: Δ histology	Similar increase in thickness (19 → 23 μm ONL thickness)	Same increase in thickness (15 → 25 μm ONL thickness)
Monotherapy: Δ ERG b-wave	**3AB/Calp/NAC**>Nec-1 (50–100 μV higher amplitudes)	**Calp/Nec-1s/NAC**>3AB (50–80 μV increase in b-wave)
Combination: Δ ERG b-wave	Smaller increase in b-wave (35 μV higher amplitudes)	Greater increase in b-wave (100 μV higher amplitudes)
Monotherapy: Δ cone density	**NAC/Nec-1s**>Calp/3AB (8 → 15 × 10^3/mm^2 = 1.87-fold inc.)	**NAC/Nec-1s**>3AB/Calp (4 →10 × 10^3/mm^2 = 2.50-fold inc.)
Combination: Δ cone density	Smaller change in density of cones (8 → 13 × 10^3/mm^2 = 1.63-fold inc.)	greater change in density of cones (4 →13 × 10^3/mm^2 = 3.25-fold inc.)
Monotherapy: Δ 30 Hz flicker	**NAC/Nec-1s**>Calp/3AB (11–14% higher amplitude)	**Nec-1s/NAC**>3AB/Calp (25% higher amplitudes)
Combination: Δ 30 Hz flicker	Smaller change in amplitude 7% higher amplitudes	Same change in amplitude (25% higher than untreated)

Drugs in bold type gave significant changes in response shown in parentheses

itself [58, 59]. Furthermore, other studies suggest that photoreceptor cell death occurs independently of microglia function [60, 61]. In the S334ter model, we observed many infiltrating microglia that actively engulfed dying rod photoreceptors, whereas in the P23H model, the cones were actively phagocytosed. We previously found that NAC treatment was very effective in inhibiting the activation of microglia in the P23H model (75% decrease in the number of microglia) which correlated with cone survival and improved visual outcome [9]. In the S334ter model, we saw a 54% decrease in the number of microglia from NAC treatment. It would be undesirable to completely block microglia function because of the homeostatic properties that are beneficial to the retina. However, targeting over-reactive microglia would reduce the production of pro-inflammatory factors. Several microglial inhibitor drugs have been tested in retinal degenerations with positive benefit including minocycline [58, 62, 63], docosahexaenoic acid [64, 65], and curcumin [65, 66]. Since both docosahexaenoic acid and curcumin were effective in the P23H model, this suggests that combination therapy for this mutation could also include a microglial inhibitor.

In conclusion, the results from this study demonstrate that more than one cellular mechanism is activated in genotype-specific retinal degeneration models. We propose that combination therapy would be the way to modulate the progression of degenerative and/or inflammatory diseases of the retina and that the specific drugs to use will depend on determining the active pathways for each genotype.

Acknowledgements This work was supported by the Canadian Institutes of Health Research Team Grant (grant number 222728 to KGE, CGE, and OLM). The authors acknowledge the use of the Wax-it Histology Service Facility, the Rodent Functional Testing Suite, and Dr. A. Gharhary at iCORD for access to the Real-Time PCR facility, all at the University of British Columbia.

Compliance with Ethical Standards

Conflict of Interest The authors declare there is no conflict of interest in the current study.

References

1. Hartong DT, Berson EL, Dryja TP (2006) Retinitis pigmentosa. Lancet 368:1795–1809
2. Berson EL (1993) Retinitis pigmentosa. The Friedenwald Lecture. Invest Ophthalmol Vis Sci 34:1659–1676
3. Sohocki MM, Daiger SP, Browne SJ, Rodriguez H, Northrup JR, Heckenlively DG et al (2001) Prevalence of mutations causing retinitis pigmentosa and other inherited retinopathies. Hum Mutat 17:42–51
4. Ripps H (2002) Cell death in retinitis pigmentosa: gap junctions and the 'bystander' effect. Exp Eye Res 74:327–336
5. Gupta N, Brown KE, Milam AH (2003) Activated microglia in human retinitis pigmentosa, late onset retinal degeneration, and age-related macular degeneration. Exp Eye Res 76:463–471
6. Komeima K, Rogers BS, Campochiaro PA (2007) Antioxidants slow photoreceptor cell death in mouse models of retinitis pigmentosa. J Cell Physiol 213:809–815
7. Punzo C, Kornacker K, Cepko CL (2009) Stimulation of the insulin/mTOR pathway delays cone death in a mouse model of retinitis pigmentosa. Nat Neurosci 12:44–52
8. Byrne LC, Dalkara D, Luna G, Fisher SK, Clerin E, Sahal JA et al (2015) Viral-mediated RdCVF and RdCVFL expression protects cone and rod photoreceptors in retinal degeneration. J Clin Invest 125:105–116
9. Viringipurampeer IA, Metcalfe AL, Bashar AE, Sivak O, Yanai Y, Mohammadi Z et al (2016) NLRP3 inflammasome activation drives bystander cone photoreceptor cell death in a P23H rhodopsin model of retinal degeneration. Hum Mol Genet 25:1501–1516
10. Rosenfeld PJ, Brown DM, Heier JS, Boyer DS, Kaiser PK, Chung CY, Kim RY, MARINA Study Group (2006) Ranibizumab for neovascular age-related macular degeneration. N Engl J Med 355:1419–1431
11. Bainbridge JW, Smith AJ, Barker SS, Robbie S, Henderson R, Balaggan K et al (2008) Effect of gene therapy on visual function in Leber's congenital amaurosis. N Engl J Med 358:2231–2239
12. Birch DG, Bennett LD, Duncan JL, Weleber RG, Pennesi ME (2016) Long-term follow-up of patients with retinitis pigmentosa receiving intraocular ciliary neurotrophic factor implants. Am J Ophthalmol 170:10–14
13. Osborne NN (2009) Recent clinical findings with memantine should not mean that the idea of neuroprotection in glaucoma is abandoned. Acta Ophthalmol 87:450–454
14. Tawbi H, Nimmagadda N (2009) Targeted therapy in melanoma. Biologics 3:475–484
15. Gulick RM, Mellors JW, Havlir D, Eron JJ, Gonzalez C, McMahon D, Richman DD, Valentine FT et al (1997) Treatment with indinavir, zidovudine, and lamivudine in adults with human immunodeficiency virus infection and prior antiretroviral therapy. N Engl J Med 337:734–739
16. Reboldi G, Gentile G, Angeli F, Verdecchia P (2009) Choice of ACE inhibitor combinations in hypertensive patients with type 2 diabetes: update after recent clinical trials. Vasc Health Risk Manag 5:411–427
17. Jadzinsky M, Pfützner A, Paz-Pacheco E, Xu Z, Allen E, Chen R, CV181-039 Investigators (2009) Saxagliptin given in combination with metformin as initial therapy improves glycaemic control in patients with type 2 diabetes compared with either monotherapy: a randomized controlled trial. Diabetes Obes Metab 11:611–622
18. Cheng JW, Li Y, Wei RL (2009) Systematic review of intraocular pressure-lowering effects of adjunctive medications added to latanoprost. Ophthalmic Res 42:99–105
19. Agarwal M, Ganesh SK, Biswas J (2006) Triple agent immunosuppressive therapy in Vogt-Koyanagi-Harada syndrome. Ocul Immunol Inflamm 14:333–339
20. Saliba RS, Munro PMG, Luthert PJ, Cheetham ME (2002) The cellular fate of mutant rhodopsin: quality control, degradation and aggresome formation. J Cell Sci 15:2907–2918
21. Noorwez SM, Kuksa V, Imanishi Y, Zhu L, Filipek S, Palczewski K, Kaushal S (2003) Pharmacological chaperone-mediated in vivo folding and stabilization of the P23H-opsin mutant associated with autosomal dominant retinitis pigmentosa. J Biol Chem 278:14442–14450
22. Oh KT, Longmuir R, Oh DM, Stone EM, Kopp K, Brown J, Fishman GA, Sonkin P et al (2003) Comparison of the clinical expression of retinitis pigmentosa associated with rhodopsin mutations at codon 347 and codon 23. Am J Ophthalmol 136:306–313

23. Dryja TP, McGee TL, Reichel E, Hahn LB, Cowley GS, Yandell DW et al (1990) A point mutation of the rhodopsin gene in one form of retinitis pigmentosa. Nature 343:364–366
24. Green ES, Menz MD, LaVail MM, Flannery JG (2000) Characterization of rhodopsin mis-sorting and constitutive activation in a transgenic rat model of retinitis pigmentosa. Invest Ophthalmol Vis Sci 41:1546–1553
25. Sandberg MA, Weigel-DiFranco C, Dryja TP, Berson EL (1995) Clinical expression correlates with location of rhodopsin mutation in dominant retinitis pigmentosa. Invest Ophthalmol Vis Sci 36: 1934–1942
26. Wasowicz M, Morice C, Ferrari P, Callebert J, Versaux-Botteri C (2002) Long-term effects of light damage on the retina of albino and pigmented rats. Invest Ophthalmol Vis Sci 43:813–820
27. Gregory-Evans K, Po K, Chang F, Gregory-Evans CY (2012) Pharmacological enhancement of ex vivo gene therapy neuroprotection in a rodent model of retinal degeneration. Ophthalmic Res 47:32–38
28. Kaur J, Mencl S, Sahaboglu A, Farinelli P, van Veen T, Ekström P et al (2011) Calpain and PARP activation during photoreceptor cell death in P23H and S334ter rhodopsin mutant rats. PLoS One 6: e22181
29. Schmittgen TD, Livak KJ (2008) Analyzing real-time PCR data by the comparative C(T) method. Nat Protoc 3:1101–1108
30. Thornberry NA, Lazebnik Y (1998) Caspases: enemies within. Science 281:1312–1316
31. Vandenabeele P, Galluzzi L, Vanden Berghe T, Kroemer G (2010) Molecular mechanisms of necroptosis: an ordered cellular explosion. Nat Rev Mol Cell Biol 11:700–714
32. Brown GC, Neher JJ (2012) Eaten alive! Cell death by primary phagocytosis: 'phagoptosis. Trends Biochem Sci 37:325–332
33. Zhao L, Zabel MK, Wang X, Ma W, Shah P, Fariss RN, Qian H, Parkhurst CN et al (2015) Microglial phagocytosis of living photoreceptors contributes to inherited retinal degeneration. EMBO Mol Med 7:1179–1197
34. Liu C, Li Y, Peng M, Laties AM, Wen R (1999) Activation of caspase-3 in the retina of transgenic rats with the rhodopsin mutation s334ter during photoreceptor degeneration. J Neurosci 19: 4778–4785
35. Arango-Gonzalez B, Trifunov D, Sahaboglu A, Michalakis S, Farinelli P, Koch F et al (2014) Identification of a common non-apoptotic cell death mechanism in hereditary retinal degeneration. PLoS One 9:e112142
36. Murakami Y, Matsumoto H, Roh M, Suzuki J, Hisatomi Y, Ikeda Y et al (2012) Receptor interacting protein kinase mediates necrotic cone but not rod cell death in a mouse model of inherited degeneration. Proc Natl Acad Sci U S A 109:14598–14603
37. Sato K, Li S, Gordon WC, He J, Liou GI, Hill JM, Travis GH, Bazan NG et al (2013) Receptor interacting protein kinase-mediated necrosis contributes to cone and rod photoreceptor degeneration in the retina lacking interphotoreceptor retinoid-binding protein. J Neurosci 33:17458–17468
38. Viringipurampeer IA, Shan X, Gregory-Evans K, Zhang JP, Mohammadi Z, Gregory-Evans CY (2014) Rip3 knockdown rescues photoreceptor cell death in blind pde6c zebrafish. Cell Death Diff 21:665–675
39. Murakami Y, Ikeda Y, Yonemitsu Y, Onimaru M, Nakagawa K, Kohno R, Miyazaki M, Hisatomi T et al (2008) Inhibition of nuclear translocation of apoptosis-inducing factor is an essential mechanism of neuroprotective activity of pigment epithelium-derived factor in a rat model of retinal degeneration. Am J Pathol 173:1326–1338
40. Zhang T, Wei Y, Jiang X, Li J, Qui S, Zhang S (2015) Protection of photoreceptors by intravitreal injection of the Y-27632 Rho-associated protein kinase inhibitor in Royal College of Surgeons rats. Mol Med Rep 12:3655–3661
41. Sanges D, Comitato A, Tammaro R, Marigo V (2006) Apoptosis in retinal degeneration involves cross-talk between apoptosis-inducing factor (AIF) and caspase-12 and is blocked by calpain inhibitors. Proc Natl Acad Sci U S A 103:17366–17371
42. Boatright JH, Moring AG, McElroy C, Phillips MJ, Do VT, Chang B, Hawes NL, Boyd AP et al (2006) Tool from ancient pharmacopoeia prevents vision loss. Mol Vis 12:1706–1714
43. Lawson EC, Bhatia SK, Han MK, Aung MH, Ciavatta V, Boatright JH et al (2016) Tauroursodeoxycholic acid protects retinal function and structure in rd1 mice. Adv Exp Med Biol 854:431–436
44. Clemson CM, Tzekov R, Krebs M, Checchi JM, Bigelow C, Kaushal S (2011) Therapeutic potential of valproic acid for retinitis pigmentosa. Br J Ophthalmol 95:89–93
45. Falsini B, Larossi G, Chiaretti A, Ruggiero A, Luigi M, Galli-Resta L et al (2016) NGF eye-drops topical administration in patients with retinitis pigmentosa, a pilot study. J Transl Med 14:8
46. Scholl HP, Moore AT, Koenekoop RK, Wen Y, Fishman GA, van den Born LI et al (2015) Safety and proof-of-concept study of oral QLT091001 in retinitis pigmentosa due to inherited deficiencies of retinal pigment epithelial 65 protein (RPE65) or lecithin:retinol acyltransferase (LRAT). PLoS One 10:e0143846
47. Kaiser WJ, Upton JW, Long AB, Livingston-Rosanoff D, Daley-Bauer LP, Hakem R, Caspary T, Mocarski ES (2011) RIP3 mediates the embryonic lethality of caspase-8-deficient mice. Nature 471: 368–372
48. Kovalenko A, Kim J-C, Kang T-B, Rajput A, Bogdanov K, Dittrich-Breiholz O, Kracht M, Brenner O et al (2009) Caspase-8 deficiency in epidermal keratinocytes triggers an inflammatory skin disease. J Exp Med 206:2161–2177
49. Orhan E, Dalkara D, Neuille M, Lechauve C, Michiels C, Picaud S et al (2015) Genotypic and phenotypic characterization of P23H line 1 rat model. PLoS One 10:e0127319
50. Sakima S, Maeda T, Bereta G, Okano K, Golczak M, Sumaroka A et al (2011) Probing mechanisms of photoreceptor degeneration in a new mouse model of the common form of autosomal dominant retinitis pigmentosa due to P23H opsin mutations. J Biol Chem 286:10551–10567
51. Chen J, Makino CL, Peachey NS, Baylor DA, Simon MI (1995) Mechanisms of rhodopsin inactivation in vivo as revealed by a COOH-terminal truncation mutant. Science 267:374–377
52. Sung C-H, Makino C, Baylor D, Nathans J (1994) A rhodopsin gene mutation responsible for autosomal dominant retinitis pigmentosa results in a protein that is defective in localization to the photoreceptor outer segment. J Neurosci 14:5818–5833
53. Hollingsworth TJ, Gross AK (2013) The severe autosomal dominant retinitis pigmentosa rhodopsin mutant Ter349Glu mislocalizes and induces rapid rod cell death. J Biol Chem 288:29047–29055
54. Sung C-H, Davenport CM, Hennessey JC, Maumenee IH, Jacobson SG, Heckenlively JR, et al (1991) Rhodopsin mutations in autosomal dominant retinitis pigmentosa. Proc Natl Acad Sci U S A 88:648l-6485
55. Thanos S (1992) Sick photoreceptors attract activated microglia from the ganglion cell layer: a model to study the inflammatory cascades in rats with inherited retinal dystrophy. Brain Res 588: 21–28
56. Noailles A, Fernández-Sánchez L, Lax P, Cuenca N (2014) Microglia activation in a model of retinal degeneration and TUDCA neuroprotective effects. J Neuroinflamm 29:176–186
57. Karlsetter M, Scholz R, Rutar M, Wong WT, Provis JM, Langmann T (2015) Retinal microglia: just bystander or target for therapy? Prog Retin Eye Res 45:30–57
58. Peng B, Xiao J, Wang K, So KF, Tipoe GL, Lin B (2014) Suppression of microglial activation is neuroprotective in a mouse model of human retinitis pigmentosa. J Neurosci 34:8139–3150

59. Zeng H, Ding M, Chen XX, Lu Q (2014) Microglial NADPH oxidase activation mediates rod cell death in the retinal degeneration in rd mice. Neuroscience 275:54–61
60. Hughes EH, Schlichtenbrede FC, Murphy CC, Broderick C, van Rooijen N, Ali RR, Dick AD (2004) Minocycline delays photoreceptor death in the rds mouse through a microglia-independent mechanism. Exp Eye Res 78:1077–1084
61. Hilla AM, Diekmann H, Fischer D (2017) Microglia are irrelevant for neuronal degeneration and axon regeneration after acute injury. J Neurosci 37:6113–6124
62. Zhang C, Lei B, Lam TT, Yang F, Sinha D, Tso MO (2004) Neuroprotection of photoreceptors by minocycline in light-induced retinal degeneration. Invest Ophthalmol Vis Sci 45:2753–2759
63. Kohno H, Chen Y, Kevany BM, Pearlman E, Miyagi M, Maeda T, Palczewski K, Maeda A (2013) Photoreceptor proteins initiate microglial activation via Toll-like receptor 4 in retinal degeneration mediated by all-trans-retinal. J Biol Chem 288:15326–15341
64. Anderson RE, Maude MB, McClellan M, Matthes MT, Yasumura D, LaVail MM (2002) Low docosahexaenoic acid levels in rod outer segments of rats with P23H and S334ter rhodopsin mutations. Mol Vis 8:351–358
65. Mirza M, Volz C, Karlsetter M, Langiu M, Somogyi A, Ruonala MO et al (2013) Progressive retinal degeneration and glial activation in the CLN6 (nclf) mouse model of neuronal ceroid lipofuscinosis: a beneficial effect of DHA and curcumin supplementation. PLoS One 8:e75963
66. Vasireddy V, Chavali VR, Joseph VT, Kadam R, Lin JH, Jamison JA et al (2011) Rescue of photoreceptor degeneration by curcumin in transgenic rats with P23H rhodopsin mutation. PLoS One 6: e21193